Report

Current Biology

Egfr Signaling Is a Major Regulator of Ecdysone Biosynthesis in the Drosophila Prothoracic Gland

Graphical Abstract

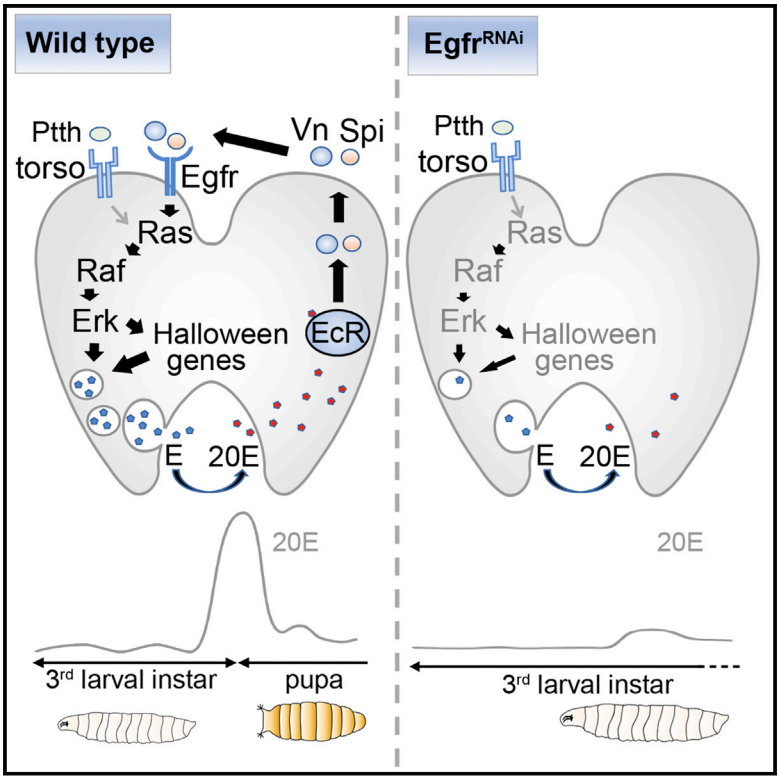

Highlights

- Egfr signaling regulates steroid hormone ecdysone biosynthesis in the PG
- Halloween gene expression and ecdysone vesicle secretion relies on Egfr pathway
- Egf ligands Vn and Spi activate Egfr signaling in the PG in an autocrine manner
- Egfr signaling and ecdysone act in a positive feedback loop circuit in the PG

Authors

Josefa Cruz, David Martín, Xavier Franch-Marro

Correspondence

david.martin@ibe.upf-csic.es (D.M.), xavier.franch@ibe.upf-csic.es (X.F.-M.)

In Brief

Levels of the steroid hormones dictate the final size of insects by triggering metamorphosis. Steroid synthesis is thought to be mainly induced by Ptth/torso signaling in the prothoracic gland. Cruz et al. now provide evidence that Egfr signaling, rather than Ptth/torso, is the major contributor of steroid biosynthesis in *Drosophila*.

Cruz et al., 2020, Current Biology *30*, 1547–1554
April 20, 2020
https://doi.org/10.1016/j.cub.2020.01.092

CellPress

Current Biology
Report

Egfr Signaling Is a Major Regulator of Ecdysone Biosynthesis in the Drosophila Prothoracic Gland

Josefa Cruz,[1] David Martín,[1,*] and Xavier Franch-Marro[1,2,*]
[1]Institute of Evolutionary Biology (IBE, CSIC-Universitat Pompeu Fabra), Passeig de la Barceloneta 37, 08003 Barcelona, Catalonia, Spain
[2]Lead Contact
*Correspondence: david.martin@ibe.upf-csic.es (D.M.), xavier.franch@ibe.upf-csic.es (X.F.-M.)
https://doi.org/10.1016/j.cub.2020.01.092

SUMMARY

Understanding the mechanisms that determine final body size of animals is a central question in biology. In animals with determinate growth, such as mammals or insects, the size at which the immature organism transforms into the adult defines the final body size, as adult individuals do not grow [1]. In *Drosophila*, the growth period ends when the immature larva undergoes the metamorphic transition to develop the mature adult [2]. This metamorphic transition is triggered by a sharp increase of the steroid ecdysone, synthetized in the prothoracic gland (PG), that occurs at the end of the third instar larvae (L3) [3–6]. It is widely accepted that ecdysone biosynthesis in *Drosophila* is mainly induced by the activation of tyrosine kinase (RTK) Torso by the prothoracicotropic hormone (Ptth) produced into two pairs of neurosecretory cells that project their axons onto the PG [7, 8]. However, the fact that neither *Ptth* nor *torso*-null mutant animals arrest larval development but only present a delay in the larva-pupa transition [9–11] mandates for a reconsideration of the conventional model. Here, we show that Egfr signaling, rather than Ptth/torso, is the major contributor of ecdysone biosynthesis in *Drosophila*. We found that Egfr signaling is activated in the PG in an autocrine mode by the EGF ligands *spitz* and *vein*, which in turn are regulated by the levels of ecdysone. This regulatory positive feedback loop ensures the production of ecdysone to trigger metamorphosis by a progressive Egfr-dependent activation of MAPK/ERK pathway, thus determining the animal final body size.

RESULTS AND DISCUSSION

In contrast to the developmental delay phenotype observed in larvae with reduced Ptth or torso, we found that specific depletion of *Drosophila* homolog transducers *ras* (*ras85D*), *Raf oncogene* (*Raf*), and *ERK*, the core components of the MAPK/ERK pathway, in the prothoracic gland (PG) using the *phmGal4* driver (*phm>*) induced developmental arrest at L3 (Figures 1A, 1B, and S1). This result suggests that additional RTKs might play important roles in ecdysone production. To study this possibility, we knocked down all known *Drosophila* RTKs in the PG and found that only depletion of *Egfr* phenocopied L3 arrested development observed in *phm* > *ras85D*^{RNAi} larvae (Figures 1A and 1B). Likewise, overexpression in the PG of a dominant-negative form of Egfr (Egfr^{DN}) or depletion of the transcription factor *pointed* (*pnt*), the principal nuclear mediator of the Egfr signaling pathway [12, 13], also resulted in arrested L3 larvae (Figures 1A and 1B). Same results were obtained upon inactivation of Egfr or different components of the MAPK/ERK pathway using an alternative PG specific driver, *amnc*^{651}*Gal4* [14] (Figure S1A). Consistent with the observed phenotypes, overexpression of a constitutively activated form of either Egfr (Egfr^{act}) or Pnt (PntP2^{Vp16}) in the PG induced premature pupariation and reduced pupal size (Figures 1B and 1C). These results are in agreement with a previous report showing that overexpression of a constitutively activated form of Ras (Ras^{V12}) in the PG produced the same phenotype [14]. Furthermore, overexpression of Ras^{V12} in Egfr-depleted larvae rescued the developmental arrest phenotype and forced premature pupation (Figures 1B and 1C). These results strongly suggest that Egfr signaling in the PG is required for the synthesis of the ecdysone pulse that triggers metamorphosis. Confirming this hypothesis, ecdysone titers in larvae depleted of either *Egfr* or *pnt* in the PG were dramatically reduced (Figure 1D). Accordingly, *Hr3* and *Hr4* expression, two direct target genes of the hormone that have been used as readouts for ecdysone levels [7, 8, 15], was completely abolished in *phm* > *Egfr*^{RNAi} and *phm* > *pnt*^{RNAi} L3 larvae compared to *control* animals (Figure 1E). Moreover, addition of the active form of ecdysone, 20-hydroxyecdysone (20E), to the food rescued the developmental arrest phenotype induced by inactivation of Egfr signaling in the PG (Figure 1F). Altogether, these results indicate that Egfr signaling in the PG endocrine cells is required for the production of the ecdysone pulse that triggers pupariation and fixes adult body size.

Since Egfr signaling is involved in cell proliferation and survival [9–11, 16–19], we analyzed whether the above-described phenotype was due to compromised viability of PG cells. Although reduced activation of Egfr signaling diminished cell size, PG cell number and viability were not affected (Figures S1B–S1D). Interestingly, ecdysone synthesis has been recently shown to correlate with endocycle progression and therefore cell size of PG cells [12, 13, 20]. PG cells undergo three rounds of endoreplication during larval development resulting in chromatin values (C values) of 32–64 C by late L3 (Figure S1E). Remarkably, we observed a clear reduction in the C value of PG cells of *phm* > *Egfr*^{RNAi} larvae at 120 h AEL, with most cells

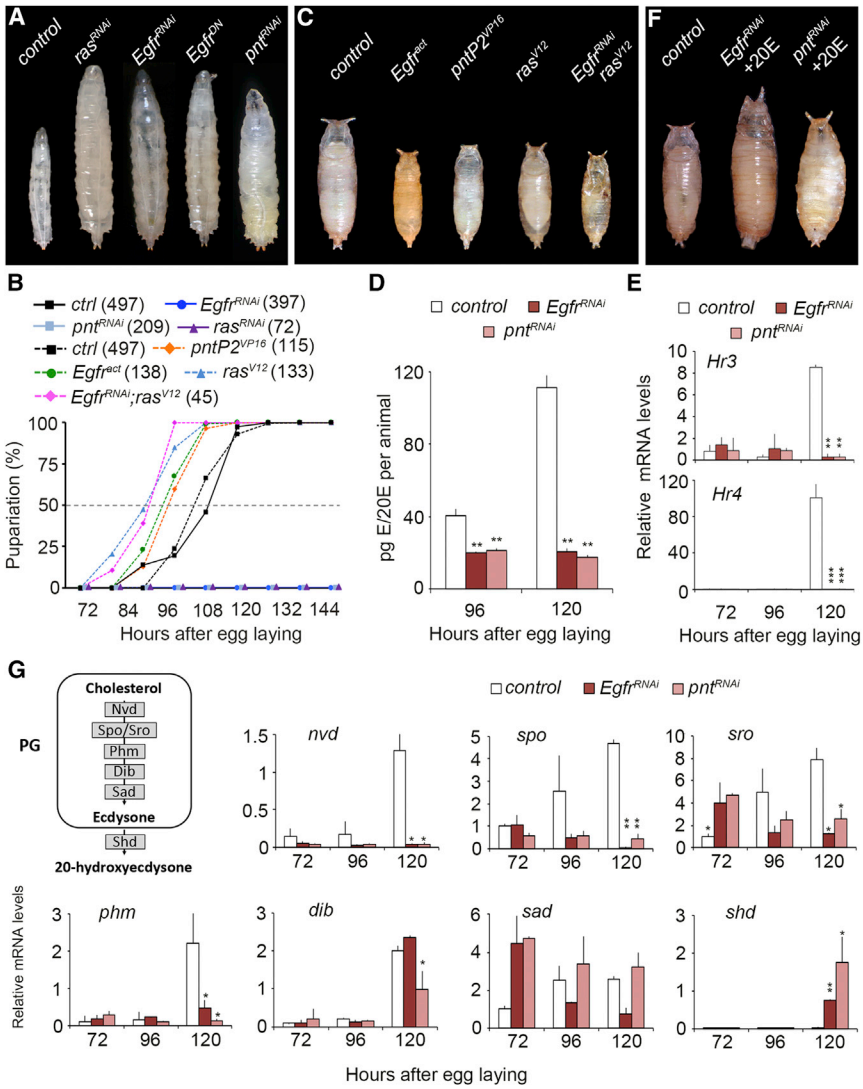

Figure 1. Disruption of Egfr Signaling Impairs Ecdysone Biosynthesis

In all experiments, *phmGal4; tubGal80ts* was used as specific PG driver (20).

(A) Compared with the control (*phmGal4; w*^{1118}), overexpression of *ras*^{RNAi}, *Egfr*^{RNAi}, *Egfr*^{DN}, and *pnt*^{RNAi} in the PG induces the arrested development of L3 larvae.

(B) Percentages of pupariated control, *Egfr*^{RNAi}, *ras*^{RNAi}, *pnt*^{RNAi}, Egfr^{act}, pntP2^{VP16}, ras^{V12}, and *Egfr*^{RNAi}; ras^{V12} animals shown at indicated stages. Numbers of animals analyzed are indicated in parenthesis.

(C) Overactivation of Egfr signaling by expressing *Egfr*^{act}, *pntP2*^{VP16}, or ras^{V12} in the PG accelerates pupariation. Expression of the constitutively active *ras*^{V12} rescues the arrested developmental of *Egfr* silencing in the PG (*Egfr*^{RNAi}; *ras*^{V12}).

(D) ELISA measurements of whole-body ecdysteroid levels in control, *Egfr*^{RNAi}, *and pnt*^{RNAi} larvae at 96 and 120 h AEL. Average values of 3 independent datasets are shown with standard errors. Statistical significance was calculated using t test (*$p < 0.05$ and **$p \leq 0.005$).

(E) mRNA levels of *Hr3* and *Hr4* of control larvae and larvae overexpressing either *Egfr*^{RNAi} or *pnt*^{RNAi} at 72, 96 and 120 h AEL, measured by qRT-PCR.

(F) Feeding with 20E rescues the arrested development induced by depletion of both *Egfr*^{RNAi} and *pnt*^{RNAi} in the PG.

(G) Schematic diagram of ecdysone biosynthetic pathway. Expression of ecdysone biosynthetic genes in control, *Egfr*^{RNAi} and *pnt*^{RNAi} larvae at 72, 96, and 120 h AEL measured using qRT-PCR. Average values of three independent datasets are shown with standard errors. Asterisks indicate differences statistically significant at *$p \leq 0.05$ and **$p \leq 0.005$ (t test).

See also Figure S1 for related results.

at 8–16 C (Figures S1E and S1F), indicating that Egfr activation is also required to promote polyploidy in the PG cells.

This result raised the possibility that Egfr signaling regulates ecdysone production by determining the size of the PG. To analyze this hypothesis, we examined the effect of Egfr signaling in ecdysone production. Steroidogenesis in the PG cells depends on the timely expression of ecdysone biosynthesis enzyme-encoding genes that mediate the conversion of cholesterol to ecdysone (Figure 1G) [14, 21]. To analyze whether Egfr signaling controls ecdysone synthesis by regulating the expression of these genes, we performed qRT-PCR in early (72 h after egg laying [AEL]), mid (96 h AEL), and late (120 h AEL) *phm* > *Egfr*^{RNAi} and *phm* > *pnt*^{RNAi} L3 larvae. Whereas expression of the six ecdysone biosynthetic genes increased gradually from mid to late L3 in *control* larvae, correlating with the production of the high-level ecdysone pulse that triggers metamorphosis [1, 22], inactivation of the Egfr pathway in the PG resulted in a dramatic reduction in the expression levels of *neverland* (*nvd*), *spook* (*spo*), *shroud* (sro), and *phantom* (*phm*) in late L3 larvae (Figure 1G). In contrast, the expression of *disembodied* (*dib*) and *shadow* (*sad*) was not significantly reduced in *Egfr*-depleted larvae, which suggests that compromising Egfr signaling in the PG does not result in a general reduction in the transcriptional activity by its minor C value, as previously shown [20], but rather by a specific transcriptional effect (Figure 1G). Further confirming this point, the overexpression of *CycE* in *Egfr*-depleted PGs was unable to restore normal expression of ecdysteroid biosynthetic genes nor induced proper pupariation of these animals (Figures S1F–S1H), indicating that Egfr signaling is required for proper expression of ecdysone enzyme-encoding genes independently of promoting polyploidy of PG cells.

As the levels of circulating ecdysone are influenced by the rates of hormone production and release, we next studied whether Egfr signaling also regulates ecdysone secretion. Recently, it has been shown that ecdysone secretion from the PG cells is mediated by a vesicular regulated transport mechanism [23]. After its synthesis, ecdysone is loaded through an ATP-binding cassette (ABC) transporter, Atet, into Syt1-positive secretory vesicles that fuse to the cytoplasmic membrane for release of the hormone in a calcium-dependent signaling [23].

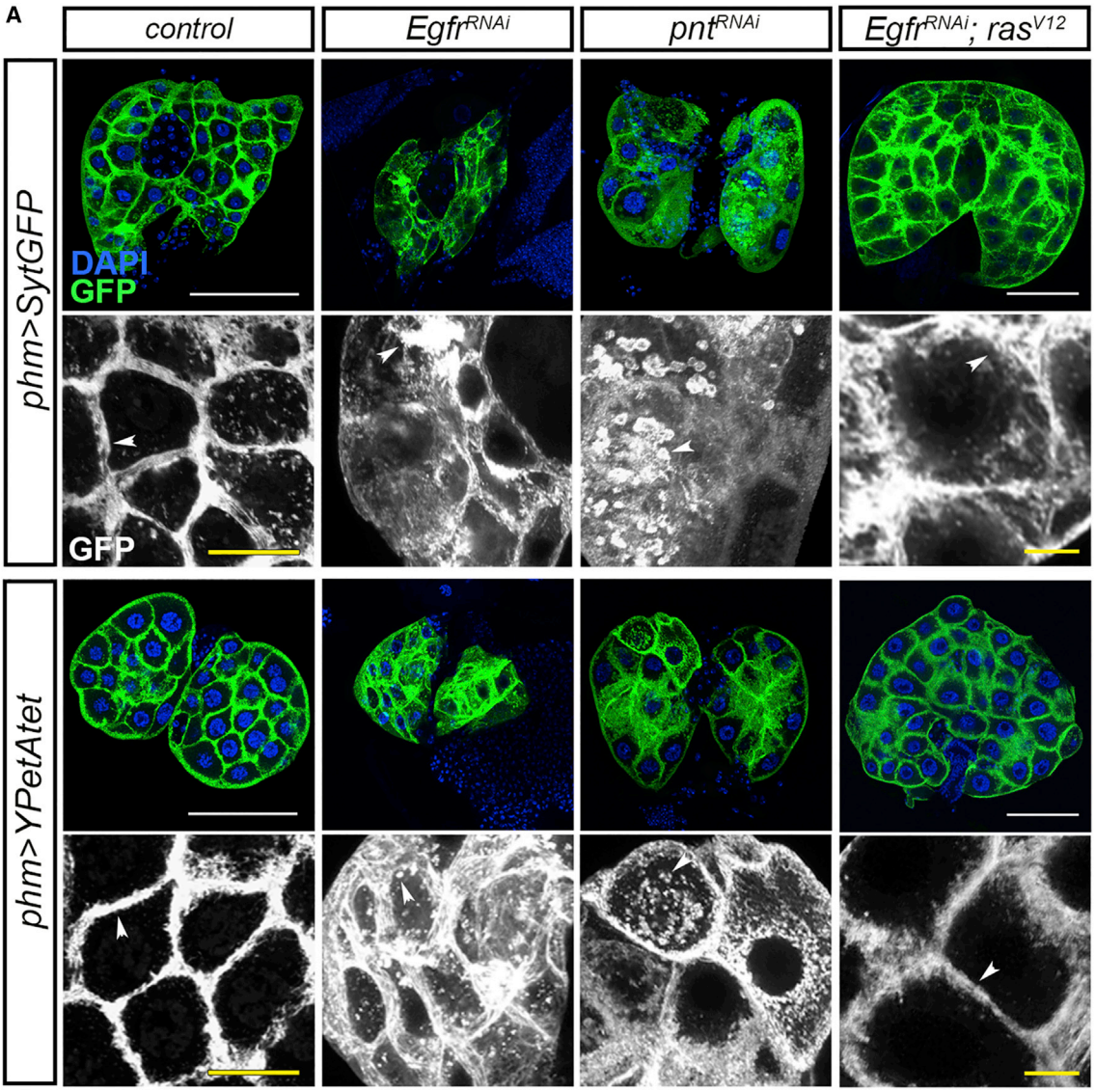

Figure 2. Egfr Signaling Regulates Ecdysone Vesicle Localization

(A) PG image of control, $Egfr^{RNAi}$, pnt^{RNAi}, and $Egfr^{RNAi}$; ras^{V12} larva at 96 h AEL overexpressing either Syt-GFP (phm^{22} > *Syt-GFP*) or YPet-Atet (phm^{22} > *YPet-Atet*). Magnified view of the PG cells shows the aggregation of small vesicle-like structures along the membrane (arrowheads). Note that compared to the control, in $Egfr^{RNAi}$ and pnt^{RNAi} PG cells vesicles accumulate in the cytoplasm. Overexpression of ras^{V12} rescues the vesicles aggregation in the cytoplasm induced by depletion *of* $Egfr^{RNAi}$. The scale bars represent 100 μm in top panels and 25 μm in magnified views. See also Figure S2 for related results.

To analyze the role of Egfr signaling in this process, we visualized secretory vesicles in PG cells of *phm* > $Egfr^{RNAi}$ and *phm* > pnt^{RNAi} L3 larvae by expressing eGFP-tagged Syt1 (Syt-GFP) in these glands [24, 25]. Whereas Syt-GFP vesicles accumulate at the plasma membrane with a small number of vesicles in the cytoplasm in wild-type L3 larval PGs, a dramatic accumulation of Syt-GFP vesicles in the cytoplasm was observed in PGs with reduced Egfr signaling (Figures 2 and S2A). Similar results were obtained when we analyzed the subcellular localization of the ecdysone transporter Atet-GFP [23] (Figures 2 and S2A). Consistently, overexpression of ras^{V12} in PGs of *phm* > $Egfr^{RNAi}$ larvae restored the subcellular localization of both Syt and Atet-GFP (Figure 2). Furthermore, mRNA levels of several genes involved in vesicle-mediated release of ecdysone [23], including *Syt* and *Atet*, were dramatically downregulated in the PG of *phm* > $Egfr^{RNAi}$ and *phm* > pnt^{RNAi} larvae (Figure S2B). Therefore, the results show that Egfr signaling is also required for the vesicle-mediated release of ecdysone from PG cells. Interestingly, direct effects of Egfr signaling on the endocytic machinery have been already described in *Drosophila* tracheal cells as well as in human cells [26–33].

The next question was to determine which of the EGF ligands were responsible for the Egfr pathway activation in the PG. In *Drosophila*, Gurken (Gur), Spitz (Spi), Keren (Krn), and Vein (Vn) serve as ligands for Egfr [34]. Expression analysis of the four ligands revealed that only *vn* and *spi* were expressed in the PGs

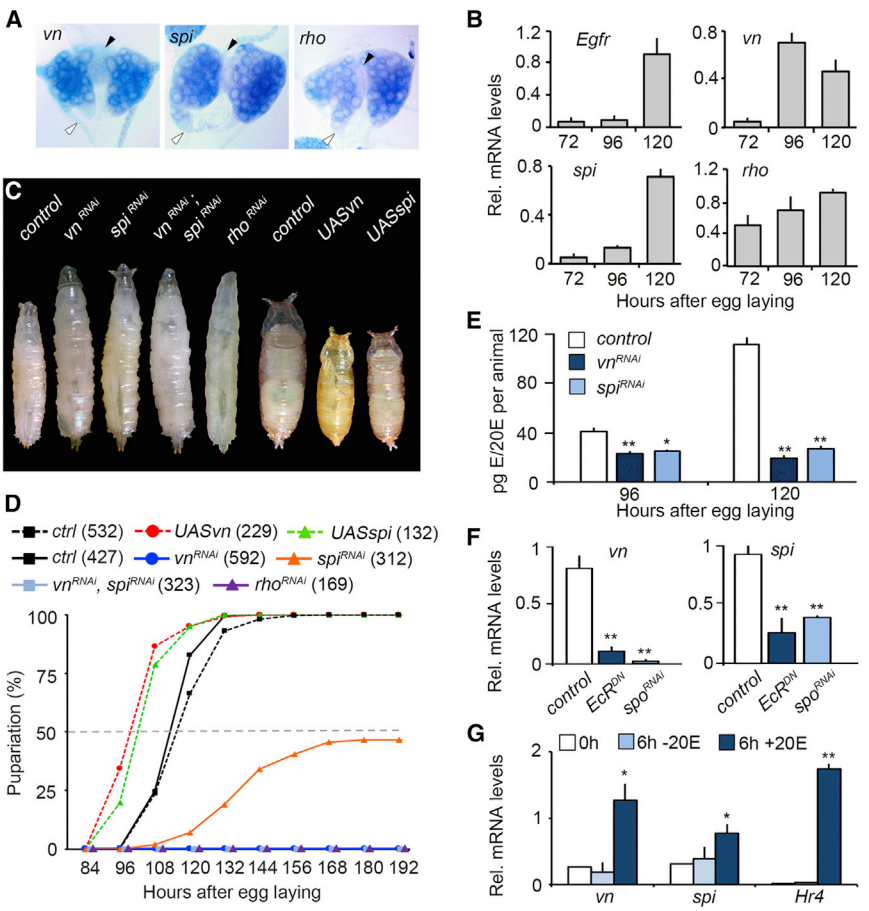

Figure 3. The Egf Ligands Vn and Spi Activate Egfr Signaling in the PG

(A) RNA *in situ* hybridization shows the expression of *vn*, *spi*, and *rho* specifically in the PG cells. Note the absence of signal in the CA (black arrowheads) and CC (white arrowheads).

(B) mRNA levels of *Egfr*, *vn*, *spi*, and *rho* of control larvae at 72, 96, and 120 h AEL, measured by qRT-PCR.

(C) Overexpression of vn^{RNAi}, spi^{RNAi}, both vn^{RNAi} and spi^{RNAi}, and rho^{RNAi} in the PG induces arrested development. In contrast, expression of either *vn* or *spi* in the PG results in accelerated pupariation and smaller pupae.

(D) Percentages of pupariated of control, *UASvn*, *UASspi*, animals reared at 18°C until early L3 and then switched to 29°C and control, rho^{RNAi}, vn^{RNAi}, spi^{RNAi} and vn^{RNAi}; spi^{RNAi} animals reared at 18°C until L2 and then switched to 29°C, shown at indicated stages. Numbers of animals analyzed are indicated in parenthesis.

(E) ELISA measurements of whole-body ecdysteroid levels in control, vn^{RNAi}, *and* spi^{RNAi} larvae at 96 and 120 h AEL. Average values of 3 independent datasets are shown with standard errors. Statistical significance was calculated using t test (*$p < 0.05$ and **$p \leq 0.005$).

(F) Expression of *vn* and *spi* of dissected ring glands (RGs) in control, *phm* > EcR^{DN}, and *phm* > spo^{RNAi} animals measured by qRT-PCR. Average values of three independent datasets are shown with standard errors. Asterisks indicate differences statistically significant at *$p \leq 0.05$ and **$p \leq 0.005$ (t test).

(G) *vn* and *spi* are activated by 20E in the ring gland. Ring glands dissected from third instar larvae at 96 and 120 AEL were cultured with and without 20E and processed for qRT-PCR measurements of *vn*, *spi*, and *Hr4*. *Hr4* was used as a positive control to the activation of the ecdysone signaling. Average values of 3 independent datasets are shown with standard errors. Statistical significance was calculated using t test (*$p < 0.05$ and **$p \leq 0.005$).

See also Figure S3 for related results.

(Figures 3A and S3A–S3D). Consistently, the intramembrane protease *rhomboid* (*rho*), which is necessary for the proteolytic activation of Spi [35], was also expressed in the PG cells (Figure 3A). A temporal expression pattern of staged L3 PGs revealed that *rho* expression progressively increased during the last larval stage, while the expression of *spi* and *vn* increased sequentially, with *vn* upregulated at mid L3 and *spi* at late L3 (Figure 3B). Consistent with the expression of the ligands, mRNA levels of *Egfr* also showed a clear upregulation by late L3 (Figures 3B and S3E). Likewise, a specific expression of PntP2 isoform was also observed in the PG of late L3 larvae (Figures S3F and S3G). Altogether, these results suggest that Vn and Spi might activate Egfr signaling in an autocrine manner to induce ecdysone production.

To determine the functional relevance of each ligand, we knocked down *vn*, *spi*, or both simultaneously in the PG. As in the case of *phm* > $Egfr^{RNAi}$, depletion of *spi*, *vn*, or both ligands at the same time caused developmental arrest in L3, although Spi appeared to have a minor effect as around 40% of *phm* > spi^{RNAi} larvae underwent delayed pupariation (Figures 3C and 3D). The attenuated effect of *spi*-depleted animals was probably due to a weaker effect of the spi^{RNAi} lines as depletion of the Spi-processing protease *rho* in the PG resulted in all *phm* > rho^{RNAi} animals arresting development at L3 (Figures 3C and 3D). Importantly, ecdysteroid levels in mid and late L3 were significantly reduced in animals depleted of either *vn* or *spi* (Figure 3E). Consistent with their role in controlling ecdysone production, overexpression of either Vn or an active-cleaved form of Spi in the PG induced precocious pupariation and smaller pupae (Figures 3C and 3D). Altogether, these findings show that *spi* and *vn* act in an autocrine manner as Egfr ligands in the PG to induce ecdysone biosynthesis during the last larval stage. In fact, the correlation between *vn* and *spi* expression with the occurrence of increasing levels of ecdysteroids points to a possible positive-feedback loop regulation with 20E inducing *vn* and *spi* expression. Consistent with this possibility, *vn* and *spi* mRNA levels were reduced in PGs of ecdysteroid deficient larvae that were generated by depleting *spo* (*phm* > spo^{RNAi}) or by overexpressing a dominant-negative form of the ecdysone receptor (*phm* > EcR^{DN}) (Figure 3F). Moreover, we cultured staged PGs for 6 h *ex vivo* in presence or absence of 20E and found that *vn* and *spi* mRNA levels were significantly upregulated in the presence of the hormone (Figure 3G). Altogether, these observations demonstrate that ecdysone exerts a positive-feedback effect on PG cells amplifying its own synthesis by inducing the expression of *vn* and *spi*. This result is consistent with a previous proposed

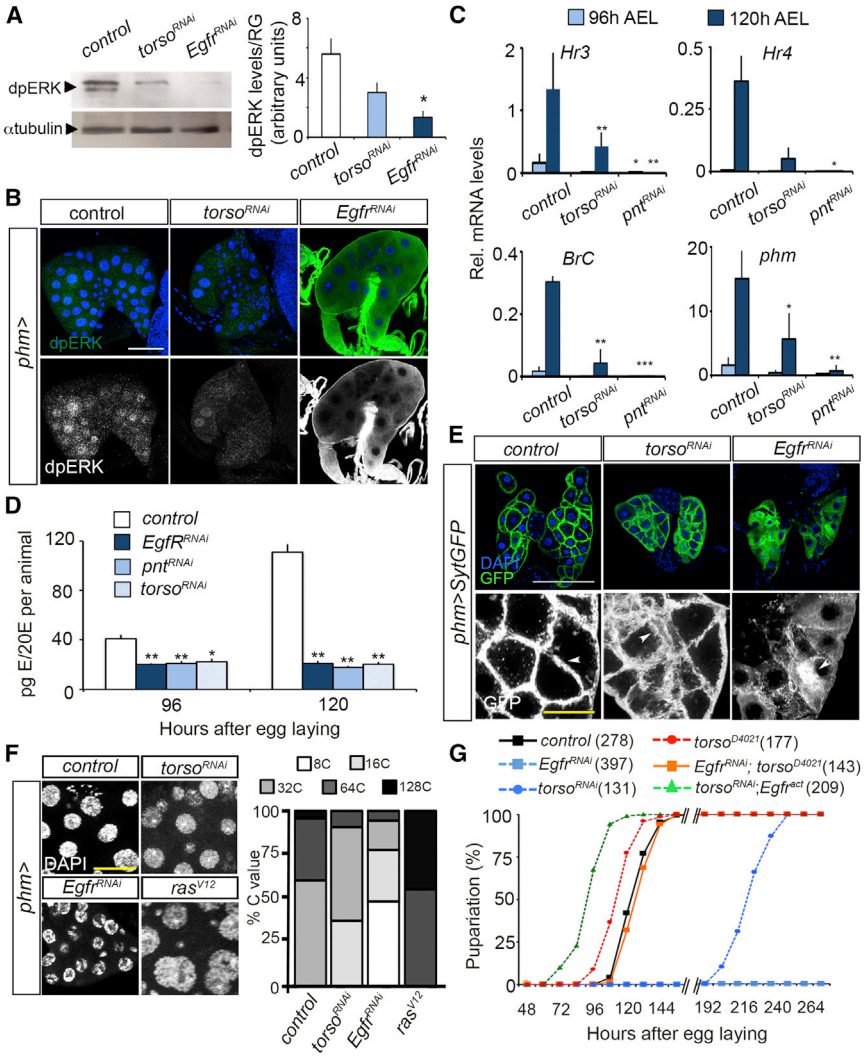

Figure 4. Progressive Activation of MAPK Cascade Induces Ecdysone Biosynthesis

(A) Quantification of diphosphorylated ERK (dp-ERK) levels in dissected RGs from L3 larvae overexpressing either *torso*^{RNAi} or *Egfr*^{RNAi}, determined by immunoblotting with an antibody specific for dp-ERK. α-tubulin was used as a loading control. dp-ERK levels are represented relative to the number of RGs. (n = 20, *p < 0.05, t test).

(B) Level of dp-ERK in the PG of control, *torso*^{RNAi}, and *Egfr*^{RNAi} L3 animals visualized by dp-ERK (in green). Nuclei are marked by DAPI (in blue). The scale bar represents 50 μm.

(C) Expression of *Hr3*, *Hr4*, *BrC*, and *phm* in dissected RGs of control and *torso*^{RNAi} and *pnt*^{RNAi} animals measured by qRT-PCR. Average values of three independent datasets are shown with standard errors. Asterisks indicate differences statistically significant at *p ≤ 0.05, **p ≤ 0.005, and ***p ≤ 0.0005 (t test).

(D) ELISA measurements of whole-body ecdysteroid levels in control, *Egfr*^{RNAi}, *pnt*^{RNAi}, *and torso*^{RNAi} larvae at 96 and 120 h AEL. Average values of 3 independent datasets are shown with standard errors. Statistical significance was calculated using t test (*p < 0.05 and **p ≤ 0.005).

(E) PG image of control, *torso*^{RNAi}, and *Egfr*^{RNAi} larva at 96 h AEL overexpressing Syt-GFP (*phm*^{22} > *Syt-GFP*). Magnified view of the PG cells shows the aggregation of small vesicle-like structures along the membrane (arrowheads) in the control and in the cytoplasm in *torso*^{RNAi} *and Egfr*^{RNAi} animals. Note that vesicle accumulation in the cytoplasm correlates with the levels of MAPK activation. The scale bars represent 100 μm in top panels and 25 μm in magnified views.

(F) Representative image of the nuclei of PG cells, marked with DAPI (in white), from control, *torso*^{RNAi}, *Egfr*^{RNAi}, and *ras*^{V12}-overexpressing larva. The scale bar represents 25 μm. Graph showing the C value of PG cells. Note that depletion of Egfr induced a major reduction of polyploidy than torso.

(G) Percentages of pupariated control, *Egfr*^{RNAi}, *torso*^{RNAi}, *torso*^{D4021}, *Egfr*^{RNAi}; *torso*^{D4021}, and *torso*^{RNAi}; *Egfr*^{act} animals shown at indicated stages. Numbers of animals analyzed are indicated in parenthesis. See also Figure S4 for related results.

model of ecdysone regulation in an autonomous mechanism by a positive feedback and biogenic amines [36, 37]. Thus, we proposed a model in which increasing levels of ecdysone promote the expression of *vn* and *spi* in the PG cells, which, in turn, increases Egfr signaling in this gland in an autocrine manner to further promote the production of ecdysone. Interestingly, it has been already shown that expression of Spi and Vn in midgut cells of *Drosophila* depends on ecdysone activity during metamorphosis [38]. In addition, in vertebrates, other hormones have been postulated to control Egfr activity, such as *Thyrotropin-releasing hormone*, which induced the phosphorylation and activation of the Egf receptor, leading to specific transcriptional events in GH3 pituitary cells [39]. Likewise, the Growth Hormone modulates Egfr trafficking and signaling by activating ERKs [40].

Thus far, the results above show that MAPK/ERK pathway is a central regulatory element in the control of ecdysone biosynthesis in the PG, with Egfr signaling chiefly contributing to its activity. However, since Ptth/torso signaling operates through the same MAPK/ERK pathway we investigated the relative contribution of this signaling pathway in the overall activity of the PG. The fact that inactivation of Egfr signaling in the PG did not affect the mRNA expression levels of either *Ptth* or *torso* (Figure S4A) points to a minor contribution of Ptth/torso signaling in the overall MAPK/ERK activity. To analyze this possibility, we compared the levels of dpERK, a readout of MAPK/ERK activity [35], in PGs of *phm* > *Egfr*^{RNAi} and *phm* > *torso*^{RNAi} larvae. As Figure 4A shows, a dramatic reduction of dpERK levels was observed in PGs of *phm* > *Egfr*^{RNAi} larvae. Importantly, dpERK levels were also reduced in *phm* > *torso*^{RNAi} PGs, although to a significant lesser extent when compared to *phm* > *Egfr*^{RNAi} larvae (Figure 4A). Similar results were observed when nuclear accumulation of dpERK was analyzed in both larvae (Figure 4B). Consistently, the level of activity of the MAPK/ERK pathway in *phm* > *pnt*^{RNAi} and *phm* > *torso*^{RNAi} larvae correlated very well with expression of the biosynthetic enzyme *phm* and the ecdysone-responsive genes *Hr3*, *Hr4*, and *Broad-Complex* (*BrC*) (Figure 4C), although the levels of ecdysone were significantly reduced in both cases

(Figure 4D). The different level of activation of dpERK by Egfr and Ptth/torso signaling was also consistent with the respective accumulation of Syt-GFP and Atet-GFP vesicles at the cytoplasm (Figures 4E and S4B) and the reduction of the C value of PG cells (Figures 4F and S4C). Finally, it is important to note that the level of activity of the MAPK/ERK pathway correlated with the respective phenotypes upon inactivation of each pathway, with *phm* > $Egfr^{RNAi}$ larvae arresting development at L3 and *phm* > $torso^{RNAi}$ larvae presenting only a delay in the pupariation time (Figure 4G). In line with this, whereas over-activation of Egfr pathway in the PG of *phm* > $torso^{RNAi}$ larvae induced a significant advancement in pupariation (Figure 4G), the expression of a constitutively activated form of Torso ($torso^{D4021}$ mutants) in PGs with depleted *Egfr* ($Egfr^{RNAi}$; $torso^{D4021}$) was not able to induce precocious pupariation (Figure 4G).

Overall, these results show that the Egfr signaling pathway plays the main role in the biosynthesis of ecdysone by activating the MAPK/ERK pathway in the PG during mid-late L3, whereas Ptth/torso signaling acts synergistically only to increase the MAPK/ERK pathway activity thus accelerating developmental timing. In this regard, it is possible that the different strength of MAPK/ERK activation by the two signaling pathways might underline this distinct requirement of each pathway. Furthermore, temporal expression of the Egfr and Torso ligands may also contribute to the difference strengths of MAPK/ERK activation, as EGF ligands *vn* and *spi* are highly expressed during L3, whereas *Ptth* is only upregulated at a specific developmental time, the wandering stage [8]. Taken together, these data suggest a model in which the increasing circulating levels of ecdysone during the last larval stage are induced by a progressive Egfr dependent activation of MAPK/ERK in the PG, whereas Ptth/torso signaling further regulates ecdysone production by integrating different environmental signals such as nutritional status, crowding conditions, and light [11]. It is important to note that, in addition to the Egfr and Ptth/torso pathways, ecdysone biosynthesis is also regulated by the insulin/insulin-like growth factor signaling (IIS)/target of Rapamycin (TOR) signaling pathway [14, 41–43]. However, in contrast to the major role of Egfr controlling ecdysteroid levels during mid-late L3, including the strong ecdysteroid pulse that triggers pupariation, the main effect of IIS/TOR pathway is to control the production of the small ecdysteroid peak that is associated to the nutrition-dependent critical weight checkpoint that occurs at the very early L3 [44]. Thus, decreasing the IIS/TOR activity in the PG delays the critical weight checkpoint, slowing development and delaying pupariation, while increasing IIS/TOR activity in the gland induces precocious critical weight and accelerates the onset of metamorphosis [14, 41–43]. Nevertheless, it is conceivable that the increasing levels of ecdysone at the critical weight checkpoint might initiate the expression of the Egf ligands, that in turn activates the ecdysone production during mid-late L3.

Finally, since no role of Ptth/torso signaling has been characterized in hemimetabolous insects, we postulate that Egfr signaling might be the ancestral ecdysone biosynthesis regulator, whereas Ptth/torso signaling has probably been co-opted in holometabolous insects during evolution to fine-tune the timing of pupariation in response to changing environmental cues. Consistent with this view, depletion of *Gb-Egfr* in the hemimetabolous insect *Gryllus bimaculatus*, where no Ptth/torso has been described, results in arrested development by the last nymphal instar [45]. Therefore, this double regulation in holometabolous insects might provide developmental timing plasticity contributing to an appropriated adaptation to a time-limited food supply.

STAR★METHODS

Detailed methods are provided in the online version of this paper and include the following:

- KEY RESOURCES TABLE
- LEAD CONTACT AND MATERIALS AVAILABILITY
- EXPERIMENTAL MODEL AND SUBJECT DETAILS
  - *Drosophila* Stocks
- METHODS DETAILS
  - Immunohistochemistry
  - *In situ* Hybridization
  - 20E Rescue Experiments
  - Raising L3 larvae for timed sample collections
  - RNA extraction and quantitative real-time reverse transcriptase polymerase chain reaction (qRT-PCR)
  - Western Blotting
  - PG Culture
  - Ecdysteroid Measurements
- QUANTIFICATION AND STATISTICAL ANALYSIS
  - DNA Quantification
  - Statistical Analysis
- DATA AND CODE AVAILABILITY

SUPPLEMENTAL INFORMATION

Supplemental Information can be found online at https://doi.org/10.1016/j.cub.2020.01.092.

ACKNOWLEDGMENTS

We thank Vienna *Drosophila* Resource Center, Bloomington *Drosophila* Stock Center for fly stocks. J. Casanova, M. O'Connor, L.A. Baena-Lopez, and S. Crossman for critical reading of the manuscript, and Silvia Chafino for technical support. We also thank the ICTS "NANOBIOSIS," and particularly the Custom Antibody Service (CAbS, IQAC-CSIC, CIBER-BBN), for the assistance in the measurement of ecdysteroids. Support for this research was provided by the Spanish MINECO (grants CGL2014-55786-P and PGC2018-098427-B-I00 to D.M. and X.F.-M.) and by the Catalan Government (2014 SGR 619 to D.M. and X.F.-M.). The research has also benefited from FEDER, UE funds.

AUTHOR CONTRIBUTIONS

Conceptualization, J.C., D.M., and X.F.-M.; Methodology, J.C., D.M., and X.F.-M.; Investigation, J.C., D.M., and X.F.-M.; Writing – Original Draft, X.F.-M.; Writing – Review & Editing, J.C., D.M., and X.F.-M.; Funding Acquisition, D.M. and X.F.-M.; Supervision, D.M. and X.F.-M.

DECLARATION OF INTERESTS

The authors declare no competing interests.

Received: June 25, 2019
Revised: December 13, 2019
Accepted: January 30, 2020
Published: March 26, 2020

REFERENCES

1. Gokhale, R.H., and Shingleton, A.W. (2015). Size control: the developmental physiology of body and organ size regulation. Wiley Interdiscip. Rev. Dev. Biol. *4*, 335–356.
2. Rewitz, K.F., Yamanaka, N., and O'Connor, M.B. (2013). Developmental checkpoints and feedback circuits time insect maturation. Curr. Top. Dev. Biol. *103*, 1–33.
3. Truman, J.W., and Riddiford, L.M. (2002). Endocrine insights into the evolution of metamorphosis in insects. Annu. Rev. Entomol. *47*, 467–500.
4. Truman, J.W., and Riddiford, L.M. (2007). The morphostatic actions of juvenile hormone. Insect Biochem. Mol. Biol. *37*, 761–770.
5. Yamanaka, N., Rewitz, K.F., and O'Connor, M.B. (2013). Ecdysone control of developmental transitions: lessons from Drosophila research. Annu. Rev. Entomol. *58*, 497–516.
6. Hiruma, K., and Kaneko, Y. (2013). Hormonal regulation of insect metamorphosis with special reference to juvenile hormone biosynthesis. Curr. Top. Dev. Biol. *103*, 73–100.
7. Gilbert, L.I., Rybczynski, R., and Warren, J.T. (2002). Control and biochemical nature of the ecdysteroidogenic pathway. Annu. Rev. Entomol. *47*, 883–916.
8. McBrayer, Z., Ono, H., Shimell, M., Parvy, J.-P., Beckstead, R.B., Warren, J.T., Thummel, C.S., Dauphin-Villemant, C., Gilbert, L.I., and O'Connor, M.B. (2007). Prothoracicotropic hormone regulates developmental timing and body size in Drosophila. Dev. Cell *13*, 857–871.
9. Rewitz, K.F., Yamanaka, N., Gilbert, L.I., and O'Connor, M.B. (2009). The insect neuropeptide PTTH activates receptor tyrosine kinase torso to initiate metamorphosis. Science *326*, 1403–1405.
10. Grillo, M., Furriols, M., de Miguel, C., Franch-Marro, X., and Casanova, J. (2012). Conserved and divergent elements in Torso RTK activation in Drosophila development. Sci. Rep. *2*, 762.
11. Shimell, M., Pan, X., Martín, F.A., Ghosh, A.C., Léopold, P., O'Connor, M.B., and Romero, N.M. (2018). Prothoracicotropic hormone modulates environmental adaptive plasticity through the control of developmental timing. Development *145*, dev159699.
12. Rutledge, B.J., Zhang, K., Bier, E., Jan, Y.N., and Perrimon, N. (1992). The Drosophila spitz gene encodes a putative EGF-like growth factor involved in dorsal-ventral axis formation and neurogenesis. Genes Dev. *6*, 1503–1517.
13. O'Neill, E.M., Rebay, I., Tjian, R., and Rubin, G.M. (1994). The activities of two Ets-related transcription factors required for Drosophila eye development are modulated by the Ras/MAPK pathway. Cell *78*, 137–147.
14. Caldwell, P.E., Walkiewicz, M., and Stern, M. (2005). Ras activity in the Drosophila prothoracic gland regulates body size and developmental rate via ecdysone release. Curr. Biol. *15*, 1785–1795.
15. King-Jones, K., and Thummel, C.S. (2005). Nuclear receptors–a perspective from Drosophila. Nat. Rev. Genet. *6*, 311–323.
16. Malartre, M. (2016). Regulatory mechanisms of EGFR signalling during Drosophila eye development. Cell. Mol. Life Sci. *73*, 1825–1843.
17. Gilboa, L., and Lehmann, R. (2006). Soma-germline interactions coordinate homeostasis and growth in the Drosophila gonad. Nature *443*, 97–100.
18. Urban, S., Brown, G., and Freeman, M. (2004). EGF receptor signalling protects smooth-cuticle cells from apoptosis during Drosophila ventral epidermis development. Development *131*, 1835–1845.
19. Bergmann, A., Tugentman, M., Shilo, B.-Z., and Steller, H. (2002). Regulation of cell number by MAPK-dependent control of apoptosis: a mechanism for trophic survival signaling. Dev. Cell *2*, 159–170.
20. Ohhara, Y., Kobayashi, S., and Yamanaka, N. (2017). Nutrient-Dependent Endocycling in Steroidogenic Tissue Dictates Timing of Metamorphosis in Drosophila melanogaster. PLoS Genet. *13*, e1006583.
21. Lavrynenko, O., Rodenfels, J., Carvalho, M., Dye, N.A., Lafont, R., Eaton, S., and Shevchenko, A. (2015). The ecdysteroidome of Drosophila: influence of diet and development. Development *142*, 3758–3768.
22. Ou, Q., Zeng, J., Yamanaka, N., Brakken-Thal, C., O'Connor, M.B., and King-Jones, K. (2016). The Insect Prothoracic Gland as a Model for Steroid Hormone Biosynthesis and Regulation. Cell Rep. *16*, 247–262.
23. Yamanaka, N., Marqués, G., and O'Connor, M.B. (2015). Vesicle-Mediated Steroid Hormone Secretion in Drosophila melanogaster. Cell *163*, 907–919.
24. Sugita, S., Han, W., Butz, S., Liu, X., Fernández-Chacón, R., Lao, Y., and Südhof, T.C. (2001). Synaptotagmin VII as a plasma membrane Ca(2+) sensor in exocytosis. Neuron *30*, 459–473.
25. Zhang, Y.Q., Rodesch, C.K., and Broadie, K. (2002). Living synaptic vesicle marker: synaptotagmin-GFP. Genesis *34*, 142–145.
26. Lanzetti, L., Rybin, V., Malabarba, M.G., Christoforidis, S., Scita, G., Zerial, M., and Di Fiore, P.P. (2000). The Eps8 protein coordinates EGF receptor signalling through Rac and trafficking through Rab5. Nature *408*, 374–377.
27. Tall, G.G., Barbieri, M.A., Stahl, P.D., and Horazdovsky, B.F. (2001). Ras-activated endocytosis is mediated by the Rab5 guanine nucleotide exchange activity of RIN1. Dev. Cell *1*, 73–82.
28. Wilde, A., Beattie, E.C., Lem, L., Riethof, D.A., Liu, S.H., Mobley, W.C., Soriano, P., and Brodsky, F.M. (1999). EGF receptor signaling stimulates SRC kinase phosphorylation of clathrin, influencing clathrin redistribution and EGF uptake. Cell *96*, 677–687.
29. Salcini, A.E., Chen, H., Iannolo, G., De Camilli, P., and Di Fiore, P.P. (1999). Epidermal growth factor pathway substrate 15, Eps15. Int. J. Biochem. Cell Biol. *31*, 805–809.
30. Zhou, Y., Tanaka, T., Sugiyama, N., Yokoyama, S., Kawasaki, Y., Sakuma, T., Ishihama, Y., Saiki, I., and Sakurai, H. (2014). p38-Mediated phosphorylation of Eps15 endocytic adaptor protein. FEBS Lett. *588*, 131–137.
31. Bryant, D.M., Kerr, M.C., Hammond, L.A., Joseph, S.R., Mostov, K.E., Teasdale, R.D., and Stow, J.L. (2007). EGF induces macropinocytosis and SNX1-modulated recycling of E-cadherin. J. Cell Sci. *120*, 1818–1828.
32. Marquèze-Pouey, B., Mailfert, S., Rouger, V., Goaillard, J.-M., and Marguet, D. (2014). Physiological epidermal growth factor concentrations activate high affinity receptors to elicit calcium oscillations. PLoS ONE *9*, e106803.
33. Bryant, J.A., Finn, R.S., Slamon, D.J., Cloughesy, T.F., and Charles, A.C. (2004). EGF activates intracellular and intercellular calcium signaling by distinct pathways in tumor cells. Cancer Biol. Ther. *3*, 1243–1249.
34. Shilo, B.-Z. (2005). Regulating the dynamics of EGF receptor signaling in space and time. Development *132*, 4017–4027.
35. Gabay, L., Seger, R., and Shilo, B.-Z. (1997). In situ activation pattern of Drosophila EGF receptor pathway during development. Science *277*, 1103–1106.
36. Moeller, M.E., Danielsen, E.T., Herder, R., O'Connor, M.B., and Rewitz, K.F. (2013). Dynamic feedback circuits function as a switch for shaping a maturation-inducing steroid pulse in Drosophila. Development *140*, 4730–4739.
37. Ohhara, Y., Shimada-Niwa, Y., Niwa, R., Kayashima, Y., Hayashi, Y., Akagi, K., Ueda, H., Yamakawa-Kobayashi, K., and Kobayashi, S. (2015). Autocrine regulation of ecdysone synthesis by β3-octopamine receptor in the prothoracic gland is essential for Drosophila metamorphosis. Proc. Natl. Acad. Sci. USA *112*, 1452–1457.
38. Li, T.-R., and White, K.P. (2003). Tissue-specific gene expression and ecdysone-regulated genomic networks in Drosophila. Dev. Cell *5*, 59–72.
39. Wang, Y.H., Jue, S.F., and Maurer, R.A. (2000). Thyrotropin-releasing hormone stimulates phosphorylation of the epidermal growth factor receptor in GH3 pituitary cells. Mol. Endocrinol. *14*, 1328–1337.
40. Huang, Y., Chang, Y., Wang, X., Jiang, J., and Frank, S.J. (2004). Growth hormone alters epidermal growth factor receptor binding affinity via activation of extracellular signal-regulated kinases in 3T3-F442A cells. Endocrinology *145*, 3297–3306.
41. Layalle, S., Arquier, N., and Léopold, P. (2008). The TOR pathway couples nutrition and developmental timing in Drosophila. Dev. Cell *15*, 568–577.
42. Colombani, J., Bianchini, L., Layalle, S., Pondeville, E., Dauphin-Villemant, C., Antoniewski, C., Carré, C., Noselli, S., and Léopold, P. (2005).

Antagonistic actions of ecdysone and insulins determine final size in Drosophila. Science *310*, 667–670.

43. Mirth, C., Truman, J.W., and Riddiford, L.M. (2005). The role of the prothoracic gland in determining critical weight for metamorphosis in Drosophila melanogaster. Curr. Biol. *15*, 1796–1807.
44. Koyama, T., Rodrigues, M.A., Athanasiadis, A., Shingleton, A.W., and Mirth, C.K. (2014). Nutritional control of body size through FoxO-Ultraspiracle mediated ecdysone biosynthesis. eLife *3*, https://doi.org/10.7554/eLife.03091.
45. Dabour, N., Bando, T., Nakamura, T., Miyawaki, K., Mito, T., Ohuchi, H., and Noji, S. (2011). Cricket body size is altered by systemic RNAi against insulin signaling components and epidermal growth factor receptor. Dev. Growth Differ. *53*, 857–869.
46. Avet-Rochex, A., Kaul, A.K., Gatt, A.P., McNeill, H., and Bateman, J.M. (2012). Concerted control of gliogenesis by InR/TOR and FGF signalling in the Drosophila post-embryonic brain. Development *139*, 2763–2772.
47. Karim, F.D., and Rubin, G.M. (1998). Ectopic expression of activated Ras1 induces hyperplastic growth and increased cell death in Drosophila imaginal tissues. Development *125*, 1–9.
48. Jiang, H., and Edgar, B.A. (2009). EGFR signaling regulates the proliferation of Drosophila adult midgut progenitors. Development *136*, 483–493.
49. O'Keefe, L., Dougan, S.T., Gabay, L., Raz, E., Shilo, B.Z., and DiNardo, S. (1997). Spitz and Wingless, emanating from distinct borders, cooperate to establish cell fate across the Engrailed domain in the Drosophila epidermis. Development *124*, 4837–4845.
50. Queenan, A.M., Ghabrial, A., and Schüpbach, T. (1997). Ectopic activation of torpedo/Egfr, a Drosophila receptor tyrosine kinase, dorsalizes both the eggshell and the embryo. Development *124*, 3871–3880.
51. Halfon, M.S., Carmena, A., Gisselbrecht, S., Sackerson, C.M., Jiménez, F., Baylies, M.K., and Michelson, A.M. (2000). Ras pathway specificity is determined by the integration of multiple signal-activated and tissue-restricted transcription factors. Cell *103*, 63–74.
52. Schindelin, J., Arganda-Carreras, I., Frise, E., Kaynig, V., Longair, M., Pietzsch, T., Preibisch, S., Rueden, C., Saalfeld, S., Schmid, B., et al. (2012). Fiji: an open-source platform for biological-image analysis. Nat. Methods *9*, 676–682.
53. McGuire, S.E., Mao, Z., and Davis, R.L. (2004). Spatiotemporal gene expression targeting with the TARGET and gene-switch systems in Drosophila. Sci. STKE *2004*, pl6.
54. Chakraborty, R., et al. (2015). Corp Regulates P53 in Drosophila melanogaster via a Negative Feedback Loop. PLoS genetics *11*, e1005400.
55. Tautz, D., and Pfeifle, C. (1989). A non-radioactive in situ hybridization method for the localization of specific RNAs in Drosophila embryos reveals translational control of the segmentation gene hunchback. Chromosoma *98*, 81–85.

STAR★METHODS

KEY RESOURCES TABLE

REAGENT or RESOURCE	SOURCE	IDENTIFIER
Antibodies		
Anti-α-Tubulin antibody, Mouse monoclonal *clone DM1A, purified from hybridoma cell culture*	Sigma-Aldrich	Cat# T6199; RRID:AB_477583
Monoclonal anti-MAP Kinase, activated (Diphosphorylated Erk-1/2) antibody produced in mouse	Sigma-Aldrich	Cat# M8159; RRID:AB_477245
Goat anti-mouse immunoglobulins/HRP polyclonal	Dako	Cat# P0447; RRID:AB_2617137
anti-PntP2 antibody produced in rat	[46]	N/A
anti-ßGalactosidase antibody produced in mouse	Developmental Studies Hybridoma Bank	Cat# 40-1a; RRID:AB_528100
Alexa Fluor 555 goat anti-rat IgG (H+L)	Molecular probes -Invitrogen	Cat# A-21434; RRID:AB_141733
Alexa Fluor 555 goat anti-mouse IgG (H+L)	Molecular probes -Invitrogen	Cat# A-21422; RRID:AB_141822
Anti-digoxin-AP Fab fragments	Roche	Cat# 11093274910; RRID:AB_514497
Chemicals, Peptides, and Recombinant Proteins		
β-Ecdysone, 2β,3β,14α,20β,22,25-Hexahydroxy-7-cholesten-6-one, Ecdysterone, Insect moulting hormone, Polypodine A	Sigma-Aldrich	Cat#: H5142
NBT/BCIP Stock Solution	Roche	Cat#: 11681451001
Formaldehyde	Sigma-Aldrich	Cat#: 1635
Ethanol	Carlo Erba reagents	Cat#: 4146072
Ribonucleic acid transfer from baker's yeast	Sigma-Aldrich	Cat#: R5636
Deionized formamide	Fluka	Cat#: 47670
Deoxyribonucleic acid sodium salt from salmon testes	Sigma-Aldrich	Cat#: D1626
Heparin sodium salt from porcine intestinal mucosa	Sigma-Aldrich	Cat#: H3393
Bovine Serum Albumin	Sigma-Aldrich	Cat#: A2153
Vectashield medium with DAPI	Vector Laboratories	Cat#: H1200
Triton X-100	United States Biochemical	Cat#: 22686
Tween-20	Sigma-Aldrich	Cat#: P9416
RQ1 DNase	Promega	Cat#: M198A
iTaq Universal SYBR Green Supermix	BioRad	Cat#: 1725121
Laemmli Sample Buffer	Bio-Rad	Cat#: 1610747
2-mercaptoethanol	Sigma-Aldrich	Cat#: M3148
Schneider's medium	GIBCO	Cat#: 21720024
Heat-inactivated fetal bovine serum	GIBCO	Cat#: 16140063
SuperSignal West Pico Chemiluminescent Substrate	ThermoScientific	Cat#: 34080
Methanol	Carlo Erba reagents	Cat#: 414814
Critical Commercial Assays		
In Situ Cell Death Detection Kit, TMR red	Roche Applied Science	Cat#: 12156792910
DIG RNA Labeling Mix	Roche	Cat#: 11277073910
20-Hydroxiecdysone ELISA kit	Bertin Bioreagents	Cat#: A05120
GenEluteMammalian Total RNA miniprepKit	Sigma-Aldrich	Cat#: RTN70
Transcriptor First Strand cDNA Synthesis kit	Roche	Cat#: 04379012001
Experimental Models: Organisms/Strains		
UAS CyE-1	Bloomington *Drosophila* Stock Center	RRID: BDSC_30725
UAS-ras85D$^{RNAi\ HMS01294}$	Bloomington *Drosophila* Stock Center	RRID: BDSC_34619
UAS-ras^{DN},	Bloomington *Drosophila* Stock Center	RRID: BDSC_4845
UAS-raf$^{RNAi\ HMC03854}$	Bloomington *Drosophila* Stock Center	RRID: BDSC_55679
UAS-raf$^{RNAi\ JF01483}$	Bloomington *Drosophila* Stock Center	RRID: BDSC_31038

(*Continued on next page*)

Continued

REAGENT or RESOURCE	SOURCE	IDENTIFIER
UAS-ERK$^{RNAi\ JF01366}$	Bloomington *Drosophila* Stock Center	RRID: BDSC_31387
UAS-Egfr$^{RNAi\ JF01368}$	Bloomington *Drosophila* Stock Center	RRID: BDSC_25781
UAS-Egfr$^{RNAi\ JF001696}$	Bloomington *Drosophila* Stock Center	RRID: BDSC_31183
UAS-Egfr$^{RNAi\ JF01083}$	Bloomington *Drosophila* Stock Center	RRID: BDSC_31525
UAS-Egfr$^{RNAi\ JF02283}$	Bloomington *Drosophila* Stock Center	RRID: BDSC_36770
UASpnt$^{RNAi\ HMS01452}$	Bloomington *Drosophila* Stock Center	RRID: BDSC_35038
UAS-rho$^{RNAi\ HMS02264}$	Bloomington *Drosophila* Stock Center	RRID: BDSC_41699
UAS-rho$^{RNAi\ JF03106}$	Bloomington *Drosophila* Stock Center	RRID: BDSC_28690
UAS-spo$^{RNAi\ HM03251}$	Bloomington *Drosophila* Stock Center	RRID: BDSC_51496
UAS-sSpi	Bloomington *Drosophila* Stock Center	RRID: BDSC_63134
Egfr-lacZ^{t1}	Bloomington *Drosophila* Stock Center	RRID: BDSC_2079
Egfr-lacZ^{k05115}	Bloomington *Drosophila* Stock Center	RRID: BDSC_10385
Egfr-lacZ	Bloomington *Drosophila* Stock Center	RRID: BDSC_61765
pnt^{1277}	Bloomington *Drosophila* Stock Center	RRID: BDSC_837
UAS-spi^{RNAi}	Vienna *Drosophila* RNAi Center	RRID: VDRC_103817
UAS-spi^{RNAi}	Vienna *Drosophila* RNAi Center	RRID: VDRC_3922
UAS-spi^{RNAi}	Vienna *Drosophila* RNAi Center	RRID: VDRC_3920
UAS-vn^{RNAi}	Vienna *Drosophila* RNAi Center	RRID: VDRC_109437
UAS-vn^{RNAi}	Vienna *Drosophila* RNAi Center	RRID: VDRC_50358
UAS-torso^{RNAi}	Vienna *Drosophila* RNAi Center	RRID: VDRC _36280
UASpnt^{RNAi}	Vienna *Drosophila* RNAi Center	RRID: VDRC_105390
Torso^{D4021}	J. Casanova	N/A
UAS-ras^{V12}	[47]	N/A
UAS-vn,	[48]	N/A
UAS-Egfr^{DN}	[49]	N/A
UAS-Egfr^{act}	[50]	N/A
UAS-pntP2^{VP16}	[51]	N/A
phm>YPetAtet	[23]	N/A
phm>SytGFP	[23]	N/A
phmGal4	Bloomington *Drosophila* Stock Center	RRID: BDSC_80577
amnc^{651}Gal4	[14]	N/A
w^{1118}	Bloomington *Drosophila* Stock Center	3605
Oligonucleotides		
See Table S1		N/A
Software and Algorithms		
Fiji	[52]	RRID: SCR 002285
Photoshop CS4	Adobe Inc.	https://www.adobe.com/
iCycler iQ Real Time PCR Detection System	Bio-Rad	https://www.bio-rad.com/
GraphPad Prism v4.00 software	GraphPad Software Inc.	RRID:SCR_002798
Microsoft Excel	Microsoft	02992-000-000010

LEAD CONTACT AND MATERIALS AVAILABILITY

Further information and requests for resources and reagents should be directed to and will be fulfilled by the lead contact, Xavier Franch-Marro (xavier.franch@ibe.upf-csic.es). This study did not generate new unique reagents

EXPERIMENTAL MODEL AND SUBJECT DETAILS

Drosophila Stocks

All fly stocks were reared on standard flour/agar *Drosophila* media at 25°C. To overexpress UAS transgenes specifically in the PG either *phmGal4* or *amnc^{651}Gal4,* kindly provided by M. O'Connor and S. Wadell respectively, were used. Conditional activation of

either RNAi or gene expression was achieved using the *Gal4/Gal80^{ts}* System [53]. In these experiments, crosses were kept at 18°C until L2 or L3 molt for conditional induction of RNAi or overexpression, respectively, when larvae were shifted to 29°C and analyzed at indicated time points. The *Drosophila* Stock Center at Bloomington, Indiana provided *UAS-CyE-1* (#30725), *UAS-ras85D^{RNAi}* HMS01294 (#34619), *UAS-ras^{DN}* (#4845), *UAS-raf* HMC03854 (#55679), *UAS-raf* JF01483 (#31038), *UAS-ERK* JF01366 (#31387), *UAS-Egfr^{RNAi}* JF01368 (#25781), *UAS-Egfr^{RNAi}* JF001696 (#31183), *UAS-Egfr^{RNAi}* JF01083 (#31525), *UAS-Egfr^{RNAi}* JF02283 (#36770), *UAS-pnt^{RNAi}* HMS01452 (#35038), *UAS-rho^{RNAi}* HMS02264 (#41699), *UAS-rho^{RNAi}* JF03106 (#28690), *UAS-spo^{RNAi}* HM03251 (#51496), *UAS-sSpi (#63134)*. *Egfr-lacZ* (#2079, #10385 and #61765) and *pnt^{1277}(pntP2-lacZ, #837)*. *UAS-spi^{RNAi}* (#103817, #3922 and #3920), *UAS-vn^{RNAi}* (#109437 and #50358), *UAS-torso^{RNAi}* (#36280), *UASpnt^{RNAi}* (#105390) were obtained from Vienna *Drosophila* RNAi Center. *Torso^{D4021}* was a kind gift from J. Casanova. *UAS-ras^{V12}* was obtained from G. Rubin. *UAS-vn* was obtained from B. Edgar. *UAS-Egfr^{DN}* was obtained from B. Shilo, *UAS-Egfr^{act}* was obtained from T. Schüpbach. *UAS-pntP2^{VP16}* was obtained from A. Michelson. *phm>YPetAtet* and *phm>SytGF*P were kindly provided by N. Yamanaka.

METHODS DETAILS

Immunohistochemistry

For fluorescent imaging, dissected ring glands (RGs) from L3 larva were dissected in 1x phosphate-buffered saline (PBS) and fixed in 4% formaldehyde or 8% for the specific detection of dpERK. RGs were rinsed in 0.1% Triton X-100 (PBST) and incubated at 4°C with primary antibodies diluted in PBST. Then, they were washed with PBST and incubated with corresponding secondary antibody (Molecular Probes, 1:500) during to 2 h at r.t. and rinsed with PBST before mounting. The following primary antibodies were used at indicated dilution: monoclonal Anti-MAP Kinase, Activated (dpERK-1&2, 1:250) antibody (Sigma-Aldrich), anti-ßGalactosidase (clone: 401.a, 1:200) from Developmental Studies Hybridoma Bank and anti-PntP2 (1:50) [46]. TUNEL labeling was performed using the TMR-Red *In Situ* Cell Death Detection Kit (Roche) according to the protocol described in a previous study [54] with minor modifications. Briefly, RGs were fixed in 4% formaldehyde, wash with PBS and permeabilized with 0.1M citrate buffer, 0.5% Triton X-100 for 5 min on ice. As a positive control, RGs were treated with DNase (Promega) for 10 min at 37°C. Samples were washed with PBS, 0.3% Triton X-100 before proceed with the TUNEL reaction. RGs were mounted in Vectashield medium with DAPI (Vector Laboratories, H1200). Images were obtained with Leica TCS SP5 confocal microscope and processed with either Fiji or Photoshop CS4 (Adobe).

In situ Hybridization

For *in situ* hybridization, dissected RGs from L3 larva were fixed in 4% formaldehyde. *in situ* hybridization was performed following the method described in a previous study [55] with minor modifications. Tissues were prehybridized in hybridization buffer (50% formamide, 5x SSC, 50ug/ul heparin, 0.1% Tween-20, 100ug/ul sonicated and denatured salmon sperm DNA, 100ug/ul tRNA from Yeast) (HS) for 3h at 55°C and RNA probes were denatured for 10min in HS at 95°C and chilled on ice. Probe hybridization was performed 0/N at 55°C. RGs were washed with a series of 3:2, 1:1 and 2:3 mixture of HS and 2xSSC, 0.1% Tween-20 (2xSSCTw) for 10 min at 55°C. Tissues were washed again at 55°C with 2xSSCTw and 0.2xSSCTw, then at r.t. with a series of 3:2 and 2:3 mixture of 0.2xSSCTw:PBTw (0.1% Tween-20 in PBS) before incubation with anti-digoxigenin-AP antibody (Roche, 1:500), diluted in 1% BSA, 0.3% Triton X-100 in PBS, O/N at 4°C. After antibody labeling, the tissues where washed with PBS, 0.3% Triton X-100 and with alkaline phosphatase buffer (100mM NaCl, 50mM MgCl2, 100mM Tris-HCl pH9.5, 0.1% Tween-20). To develop color reaction, samples where incubated with NBT/BCIP (Roche) solution in dark for 30min to 1h. *vn*, *spi*, *Krn* and *rho* probes were generated from DNA fragments amplified by PCR from genomic DNA with specific primers and digoxigenin-labeled RNA probes were generated by *in vitro* transcription following the manufacturer's instructions (DIG RNA Labeling Mix, Roche). Images were obtained with the Zeiss microscope.

20E Rescue Experiments

20E (Sigma, H5142) was dissolved in ethanol at 5mg/ml. Standard flour-agar medium was supplemented with 0,35 mg/ml of the hormone or an equal amount of ethanol. For rescue experiments, embryos were collected after L3 molt and reared on 20E-supplemented medium or control medium with ethanol. *phm > w^{1118}* was used as a control.

Raising L3 larvae for timed sample collections

Larvae were synchronized by allowing flies to lay eggs at 25°C for 4h on agar plates supplemented with yeast paste. Between 25 to 30 freshly eclosed L1 larvae were collected and transferred to vials and incubated at 18°C until L2 or L3 molting and then shifted to 29°C. The time and date of pupariation were scored every 1-5 h during the light cycle and the time in hours. Data from 8-10 vials were put together and ordered by pupariation time and cumulative percentage pupariation and subsequently analyzed in Microsoft Excel.

RNA extraction and quantitative real-time reverse transcriptase polymerase chain reaction (qRT-PCR)

Total RNA was isolated with the GenElute^{TM} Mammalian Total RNA kit (Sigma), DNase treated (Promega) and reverse transcribed with Transcriptor First Strand cDNA Synthesis kit (Roche, #04379012001). Relative transcripts levels were determined by real-time PCR (qPCR), using iTaq Universal SYBR Green Supermix (Bio-Rad). To standardize the qPCR inputs, a master mix that contained iTaq Universal SYBR Green PCR Supermix and forward and reverse primers was prepared (final concentration: 100nM/qPCR). The qPCR experiments were conducted with the same quantity of tissue equivalent input for all treatments and each sample

was run in duplicate using 2 μl of cDNA per reaction. All the samples were analyzed on the iCycler iQ Real Time PCR Detection System (Bio-Rad). For each standard curve, one reference DNA sample was diluted serially. RNA expression was calculated in relation to the expression of Rpl32.

Western Blotting

40 RGs were dissected in cold PBS and transferred to 40 μl Laemmli Sample Buffer (Bio-Rad, 1610747) supplemented with 2-mercaptoethanol. Samples were boiled for 5 minutes, centrifuged at 14,000 g and 20 μl supernatant were loaded in duplicate on a 10% polyacrylamide gel followed by transfer onto a PVDF membrane (Millipore). The membrane was incubated with PBS, 0.05% Tween-20, 5% nonfat dry milk (PBSTwM) O/N at r.t. with gentle agitation, then whashed with PBSTw at r.t. Membrane was cut in half, and each samples replicate was incubated with the corresponding primary antibody O/N at 4°C. Mouse anti-alfa-Tubulin DM1A, 1:1000 (Sigma, #T6199) antibody was used as a loading control and mouse anti-phospho-ERK, 1:2000 (Sigma, #M8159) antibody to detect the levels of dpERK. Membranes were washed with 0.05% PBSTw at r.t for 2h. Secondary antibody incubation was performed at r.t. for 2h, then, the membrane was washed with 0.05% PBSTw at r.t prior to signal development with SuperSignal West Pico Chemiluminescent Substrate (ThermoScientific, #34080). Secondary antibody Goat anti-mouse immunoglobulins/HRP polyclonal, 1:2000 (Dako, #P0447) were used. The blot was scanned on an Odessey Fc (LI-COR) and Fiji, was used for image processing and protein quantification.

PG Culture

RGs from 80h AEL larvae reared at 25°C, were dissected in PBS. Dissected ring glands from 10 animals per each replicate were cultured at 25°C in Schneider's medium (GIBCO, #21720024) supplemented with 10% heat-inactivated fetal bovine serum (GIBCO, #16140063) for one hour, before transferring them to fresh medium supplemented with $5x10^{-6}$M of 20E (Sigma Aldrich, #H5142) dissolved in 10% ethanol, or with the same volume of 10% ethanol. Samples were processed for qRT-PCR after 6 hours in culture.

Ecdysteroid Measurements

Fifteen staged third instar larvae were preserved in 500ul of methanol. Samples were homogenized and centrifuged (10cmin at 18c000 × *g*). The remaining tissue was re-extracted twice in 0.5 mL methanol and the resulting methanol supernatants were dried using a SpeedVac. Samples were resuspended in enzyme immunoassay buffer (0.4cM NaCl, 1cmM EDTA, 0.1% bovine serum albumin in 0.1 M phosphate buffer). ELISA was performed according to the manufacturer's instructions using a commercial ELISA kit (Bertin Bioreagents) that detects ecdysone and 20-hydroxyecdysone with the same affinity. Absorbance was measured at 405 nm on a plate reader, SpectramaxPlus (Molecular Devices, Sunnyvale, CA) using GraphPad Prism v4.00 software (GraphPad Software Inc., San Diego, CA).

QUANTIFICATION AND STATISTICAL ANALYSIS

DNA Quantification

For DNA quantification, DNA staining intensity in the PG cells was obtained from z stacked images of DAPI stained L3 larvae. DNA staining intensity of PG cells was normalized using average DNA staining intensity of the diploid cells of Tr2 tracheal system. Thus, the C value of PG nucleus was set as DNA staining intensity in the tracheal cells of Tr2/DNA staining intensity in PG. Images were obtained with Leica SP5 confocal microscope. A series of 2D images were taken every 0.25 μm slices. Image analysis was performed using Fiji.

Statistical Analysis

Experiments were performed with three biological replicates. At qPCR experiments, each biological replicate corresponds to 10 whole larvae, in Figures 1G, S1H, and S4A and 20 RGs in all other experiments. The biological replicates for ecdysteroids measurements in ELISA quantification corresponds to 15 whole larvae. The average and standard error mean were represented. Two-tailed Student's test was performed to determine which values were significantly different. Asterisks indicate differences statistically significant at $p \leq 0.05$ (*), and $p \leq 0.005$ (**). The sample size for pupariation time and cumulative pupariation percentage is indicated at the corresponding figure.

DATA AND CODE AVAILABILITY

This study did not generate any new computer code or algorithms. Raw images used for quantitative analyses are available form the lead author upon request.